

Prediction of the turning and zig-zag maneuvering performance of a surface combatant with URANS

Suleyman Duman¹ and Sakir Bal^{*2}

¹Department of Naval Architecture and Marine Engineering, Yildiz Technical University, Istanbul, Turkey

²Department of Naval Architecture and Marine Engineering, Istanbul Technical University, Istanbul, Turkey

(Received March 16, 2017, Revised November 20, 2017, Accepted November 25, 2017)

Abstract. The main objective of this study is to investigate the turning and zig-zag maneuvering performance of the well-known naval surface combatant DTMB (David Taylor Model Basin) 5415 hull with URANS (Unsteady Reynolds-averaged Navier-Stokes) method. Numerical simulations of static drift tests have been performed by a commercial RANS solver based on a finite volume method (FVM) in an unsteady manner. The fluid flow is considered as 3-D, incompressible and fully turbulent. Hydrodynamic analyses have been carried out for a fixed Froude number 0.28. During the analyses, the free surface effects have been taken into account using VOF (Volume of Fluid) method and the hull is considered as fixed. First, the code has been validated with the available experimental data in literature. After validation, static drift, static rudder and drift and rudder tests have been simulated. The forces and moments acting on the hull have been computed with URANS approach. Numerical results have been applied to determine the hydrodynamic maneuvering coefficients, such as, velocity terms and rudder terms. The acceleration, angular velocity and cross-coupled terms have been taken from the available experimental data. A computer program has been developed to apply a fast maneuvering simulation technique. Abkowitz's non-linear mathematical model has been used to calculate the forces and moment acting on the hull during the maneuvering motion. Euler method on the other hand has been applied to solve the simultaneous differential equations. Turning and zig-zag maneuvering simulations have been carried out and the maneuvering characteristics have been determined and the numerical simulation results have been compared with the available data in literature. In addition, viscous effects have been investigated using Eulerian approach for several static drift cases.

Keywords: ship maneuvering; turning circle; zig-zag maneuver; CFD (Computational Fluid Dynamics); DTMB 5415; drift; wave deformations; hydrodynamic derivatives; viscous effects

1. Introduction

Performance predictions of ship-maneuvering have been a vital subject for decades in naval hydromechanics. The assessment of ship-maneuvering performance in the early design stage has a significant role to get sufficient adequacy of ship's controllability. In order to estimate the ship-maneuvering performance, experimental, numerical and empirical methods have been widely used in the past. As it is known, the experimental methods are expensive and time consuming. Meanwhile, numerical methods are cost effective as compared with the experiments and are

*Corresponding author, Professor, E-mail: sbal@itu.edu.tr

quick-responding methods. In addition, CFD (Computational Fluid Dynamics) methods can be employed for both simulating viscous and inviscid flows.

Although the potential flow computations have been used in the prediction of ship resistance (Bal 2008, Uslu and Bal 2008) and analysis of a WIG (wing-in-ground) moving over the free water surface (Bal 2016), viscous CFD codes have become more reliable and efficient in ship maneuvering problems. CFD based methods has been exercised extensively for ship hydrodynamic problems, e.g., ship resistance predictions, static and dynamic maneuvers (Simonsen and Stern 2003, Bhushan *et al.* 2007, Sakamoto 2009, Kim *et al.* 2015, Kinaci *et al.* 2016, Hajivand and Mousavizadegan 2015). The scale effects in ship resistance and maneuvering characteristics have been studied by using numerical approach (Nikolaev and Lebedeva 1980, Duman and Bal 2016b).

The CFD simulations provide more insights to the entire flow structure around the hull, and the forces and moments acting on the hull can be computed by integrating the properties of the fluid particles around the hull (Yoon 2009). Hydrodynamic derivatives then can be calculated by using the numerical simulation results. However, there are some difficulties of RANS approach, such as, the implementation of complex geometries, solving 6-DOF (degrees-of-freedom) ship motions (needs huge computing capability) and environmental effects etc. Moreover, RANS methods are required to be verified and validated (Stern *et al.* 2001) to be reliable and accepted by end-users as a solution tool for use in industry or the navy.

Recently, international workshops have been organized via collaboration of related institutions. Researches about the ship-maneuvering have focused on modern tankers (KVLCC1 and KVLCC2), Kreso Container Ship (KCS), and US Navy surface combatant (DTMB 5415), which is currently used in this study. In the Gothenburg 2000 Workshop, Larsson *et al.* (2003) and Kim *et al.* (2001) provided steady-flow data for KCS and KVLCC2. For DTMB 5415, data procurement has been part of an international collaboration between IIHR (Iowa Institute of Hydraulic Research), INSEAN (Italian Ship Model Basin) and DTMB (David Taylor Model Basin), for more than 10 years (Yoon 2009). After the Gothenburg Workshop, SIMMAN 2008 and SIMMAN 2014 Workshops were organized to discuss more recent studies.

A commonly used method to predict the ship maneuvering performance is to simulate standard maneuvers by solving the equations of motion with experimentally or numerically determined maneuvering coefficients which was proposed by Abkowitz (1964). Once these coefficients are determined for a specific ship, the equations of motion can be solved simultaneously to simulate the dynamic behavior of the ship. Another mathematical model to represent the hydrodynamic forces and moments was proposed by the Japanese Mathematical Modeling Group (MMG) in the late 1970s last century. According to this model, forces and moments are separated into several parts such as; hull, propeller and rudder etc. (Yoshimura *et al.* 2005). The main objective of this research is to investigate the turning and zig-zag maneuvering characteristics of the US Navy surface combatant DDG51 guided missile destroyer in 1/46.588 model scale ratio by performing several URANS simulations. The model used for this purpose is 5512, a length of 3.048 m and a geosim of DTMB 5415. Numerical simulations of static drift tests have been conducted by using a commercial RANS solver software Star-CCM+ based on the finite volume method (FVM) in an unsteady manner in order to determine the maneuvering characteristics of the model. The model is un-appended except for port and starboard bilge keels, i.e., not equipped with shaft, struts, propellers, or rudders as is used in PMM tests at IIHR (Yoon *et al.* 2015). First, the numerical method has been validated for un-appended model. After validation of the method, rudders have been implemented to the model in order to calculate the rudder coefficients. In addition, inviscid

simulations have been carried out for several static drift cases and the results are compared with those of viscous model, via forces and moments acting on the hull (Duman and Bal 2016a).

A computer program has been developed in order to apply a fast simulation technique. Abkowitz's nonlinear mathematical method has been adopted to calculate the forces and moment acting on the hull during the maneuvering motion. The angular velocity, acceleration and cross-coupled terms have been taken from the available data in literature. Euler method has been used to solve simultaneous differential equations of ship maneuvering motion (Duman 2016). The rudder deflection, principal particulars of the ship model and hydrodynamic derivatives have been used as inputs to the program. Turning and zig-zag maneuvering simulations have been carried out and the maneuvering characteristics have then been determined. The results of oblique towing CFD simulations and the maneuvering characteristics obtained by the fast-time maneuvering simulations have been compared with the available experimental data in literature.

2. Mathematical model- Ship maneuvering equations

The generalized 6-DOF rigid-body equations of motion in a body-fixed, non-inertial frame of reference xyz that is moving relative to an Earth-fixed inertial reference frame $x_0y_0z_0$ can be derived as followed (Fossen 1994)

$$\begin{aligned}
 m\left[\dot{u} - vr + \omega q - x_G(q^2 + r^2) + y_G(pq - \dot{r}) + z_G(pr + \dot{q})\right] &= X \\
 m\left[\dot{v} - \omega p + ur - y_G(r^2 + p^2) + z_G(qr - \dot{p}) + x_G(qp + \dot{r})\right] &= Y \\
 m\left[\dot{\omega} - uq + vp - z_G(p^2 + q^2) + x_G(rp - \dot{q}) + y_G(rq + \dot{p})\right] &= Z \\
 I_x\dot{p} + (I_z - I_y)qr - (\dot{r} + pq)I_{xz} + (r^2 - q^2)I_{yz} + (pr - \dot{q})I_{xy} \\
 + m\left[y_G(\dot{\omega} - uq + vp) - z_G(\dot{v} - \omega p + ur)\right] &= K \quad (1) \\
 I_y\dot{q} + (I_x - I_z)rp - (\dot{p} + qr)I_{xy} + (p^2 - r^2)I_{zx} + (qp - \dot{r})I_{yz} \\
 + m\left[z_G(\dot{u} - vr + \omega q) - x_G(\dot{\omega} - uq + vp)\right] &= M \\
 I_z\dot{r} + (I_y - I_x)pq - (\dot{q} + rp)I_{yz} + (q^2 - p^2)I_{xy} + (rq - \dot{p})I_{zx} \\
 + m\left[x_G(\dot{v} - \omega p + ur) - y_G(\dot{u} - vr + \omega q)\right] &= N
 \end{aligned}$$

The first three equations represent the translational motion; surge- x , sway- y and heave- z while the last three equations represent the rotational motions; roll- ϕ , pitch- θ and yaw- ψ , respectively.

The origin of ship-fixed reference frame is located at the gravity center of the ship (Fig. 1). Right hand side (RHS) of the 6-DOF equations of motion represents the forces and moments; X , Y , Z are the external forces acting on the ship and K , M , N are the external moments where m is the mass of the ship and I_x , I_y , I_z are the moments of inertia with respect to each axis. The center of gravity of the ship is given at the point defined with x_G , y_G , z_G on the earth-fixed reference frame.

For surface ships moving on unbounded calm water, forces and moments acting on the hull are in the horizontal plane. Hence, the heave, roll and pitch motions can be neglected such that $\omega = p = q = \dot{\omega} = \dot{p} = \dot{q} = 0$. Due to symmetry of the vessel in the xz -plane, $y_G = 0$. The equations of motion for surface ships take the following form when these simplifications are made.

$$\begin{aligned}
 m(\dot{u} - vr - x_G r^2) &= X \\
 m(\dot{v} + ur + x_G \dot{r}) &= Y \\
 I_z \dot{r} + mx_G(\dot{v} + ur) &= N
 \end{aligned}
 \tag{2}$$

X , Y , N represent the surge, sway forces and yaw moment in the ship-fixed coordinate system, respectively.

There are two kinds of approaches for expression of the hydrodynamic forces and moment during the maneuvering motion of ships, one is that introduced first by Abkowitz (1964) and the other one is the Mathematical Model Group (MMG) (Yoshimura 2005). Abkowitz (1964) proposed a method for expression of the hydrodynamic forces and moment acting on the hull by using nonlinear approximation. These forces and moment are expressed as functions of the kinematic parameters and the rudder deflection angle in the following form.

$$\begin{aligned}
 X &= F_x(u, v, r, \dot{u}, \dot{v}, \dot{r}, \delta) \\
 Y &= F_y(u, v, r, \dot{u}, \dot{v}, \dot{r}, \delta) \\
 N &= N(u, v, r, \dot{u}, \dot{v}, \dot{r}, \delta)
 \end{aligned}
 \tag{3}$$

For simplicity, the hydrodynamic derivatives can be written in the following form (Nomenclature 1952)

$$\frac{\partial X}{\partial u} = X_u, \quad \frac{\partial X}{\partial v} = X_v, \quad \frac{\partial X}{\partial \dot{u}} = X_{\dot{u}}, \quad \frac{\partial X}{\partial \delta} = X_{\delta}, \quad \frac{\partial^2 X}{\partial u^2} = X_{uu}, \quad \frac{\partial^2 X}{\partial v \partial u} = X_{uv} \text{ etc.} \tag{4}$$

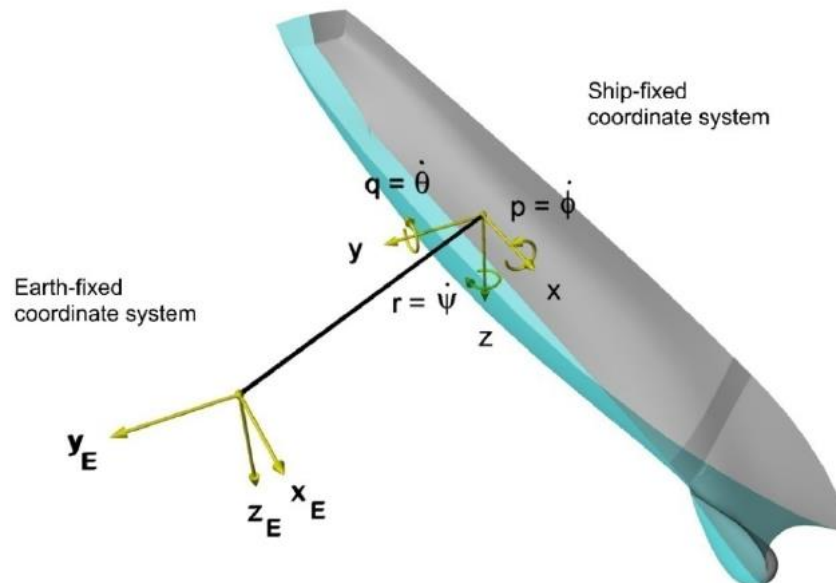


Fig. 1 Earth and ship fixed coordinate systems (Yoon 2009)

If the functions in Eq. (3) are expanded into Taylor Series about the initial steady state of forward motion with constant speed, i.e., $u_0 = U$, $v_0 = 0$, $\dot{u}_0 = 0$, $\dot{v}_0 = 0$, $r_0 = 0$, $\dot{r}_0 = 0$, $\delta_0 = 0$, the following expressions can be found,

$$\begin{aligned}
X &= X_0 + X_{\dot{u}}\dot{u} + X_u(\Delta u) + X_{uu}(\Delta u)^2 + X_{uuu}(\Delta u)^3 + X_{vv}v^2 + X_{rr}r^2 + X_{\delta\delta}\delta^2 \\
&\quad + X_{vuu}v^2(\Delta u) + X_{rru}r^2(\Delta u) + X_{\delta\delta u}\delta^2(\Delta u) + X_{vr}vr + X_{v\delta}v\delta + X_{r\delta}r\delta + X_{vru}vr(\Delta u) \\
&\quad + X_{v\delta u}v\delta(\Delta u) + X_{r\delta u}r\delta(\Delta u) \\
Y &= Y_0 + Y_u(\Delta u) + Y_{uu}(\Delta u)^2 + Y_{uuu}(\Delta u)^3 + Y_{\dot{v}}\dot{v} + Y_vv + Y_{vv}v^2 + Y_{vvv}v^3 + Y_{vrr}vr^2 + Y_{v\delta\delta}v\delta^2 \\
&\quad + Y_{vu}v(\Delta u) + Y_{vuu}v(\Delta u)^2 + Y_{\dot{r}}\dot{r} + Y_r r + Y_{rr}r^2 + Y_{rvv}rv^2 + Y_{r\delta\delta}r\delta^2 + Y_{ru}r(\Delta u) + Y_{ruu}r(\Delta u)^2 \\
&\quad + Y_{\delta}\delta + Y_{\delta\delta\delta}\delta^3 + Y_{\delta vv}\delta v^2 + Y_{\delta rr}\delta r^2 + Y_{\delta u}\delta(\Delta u) + Y_{\delta uu}\delta(\Delta u)^2 + Y_{\delta\delta\delta u}\delta^3(\Delta u) + Y_{vr\delta}vr\delta \\
N &= N_0 + N_u(\Delta u) + N_{uu}(\Delta u)^2 + N_{uuu}(\Delta u)^3 + N_{\dot{v}}\dot{v} + N_vv + N_{vv}v^2 + N_{vvv}v^3 + N_{vrr}vr^2 \\
&\quad + N_{v\delta\delta}v\delta^2 + N_{vu}v(\Delta u) + N_{vuu}v(\Delta u)^2 + N_{\dot{r}}\dot{r} + N_r r + N_{rr}r^2 + N_{rvv}rv^2 + N_{r\delta\delta}r\delta^2 \\
&\quad + N_{ru}r(\Delta u) + N_{ruu}r(\Delta u)^2 + N_{\delta}\delta + N_{\delta\delta\delta}\delta^3 + N_{\delta vv}\delta v^2 + N_{\delta rr}\delta r^2 + N_{\delta u}\delta(\Delta u) \\
&\quad + N_{\delta uu}\delta(\Delta u)^2 + N_{\delta\delta\delta u}\delta^3(\Delta u) + N_{vr\delta}vr\delta
\end{aligned} \tag{5}$$

X_0 , Y_0 and N_0 are the steady state values of X , Y , N , respectively. Δu is the disturbance in surge velocity. Each term represents a maneuvering coefficient that is used in the Abkowitz's mathematical model. In order to generalize the problem and to make easy for studying the influence of parameters, it is convenient to non-dimensionalize the ship-maneuvering motion equations. The procedure in the prime system of SNAME has been applied (Nomenclature 1952).

According to this system, L , L/V and $1/2\rho L^2T$ are used as the dimensions for length, time and mass, respectively, where the L is the length of the ship, V is the ship advance speed, ρ is the density of water and T is the draught of the ship.

3. Computational method

All computations in this study have been performed using the RANS solver software Star-CCM+ from CD-adapco. The software is based on a finite volume method. Appropriate initial boundary conditions and a number of discrete approximations are needed to obtain an algebraic equation system solvable on a computer. First, the computational domain is subdivided into a finite number of control volumes which have fully hexahedral shape in this study. The total solution time is also subdivided into time steps according to ITTC CFD recommendations.

The fluid flow is considered as 3-D, incompressible, transient and fully turbulent. Hydrodynamic analyses have been carried out for Froude number 0.28. During the analyses, the free surface effects have been taken into account using VOF method (Hirt and Nichols 1981) which is utilized by Eulerian fluid approach and hull is considered as fixed. The flow is assumed to be governed by the RANS equations, in which turbulence effects are included via two-equation model. Thus, the continuity equation, three momentum equations and two equations for turbulence are solved. Wall function is employed to represent the flow near the boundaries. It is activated when the non-dimensional wall distance (y^+) becomes in the range of 30-300. In this study, y^+ values are between 40-50.

3.1 Governing equations

Considering the flow incompressible with constant viscosity and assume that there are no body forces acting on the hull, the averaged continuity and momentum equations may be written in tensor form and Cartesian coordinates as follows (Ferziger and Perić 2002).

$$\frac{\partial(\rho\bar{u}_i)}{\partial x_i} = 0 \quad (6)$$

$$\frac{\partial(\rho\bar{u}_i)}{\partial x_i} + \frac{\partial(\rho\bar{u}_i\bar{u}_j + \rho\bar{u}_i\bar{u}_j')}{\partial x_j} = -\frac{\partial\bar{p}}{\partial x_i} + \frac{\partial\bar{\tau}_{ij}}{\partial x_i} \quad (7)$$

in which $\bar{\tau}_{ij}$ are the mean viscous stress tensor components, as shown in Eq. (8)

$$\bar{\tau}_{ij} = \mu \left(\frac{\partial\bar{u}_i}{\partial x_j} + \frac{\partial\bar{u}_j}{\partial x_i} \right) \quad (8)$$

and p is the mean pressure, \bar{u}_i is the average Cartesian components of the velocity vector, $\rho\bar{u}_i\bar{u}_j'$ is the Reynolds stresses, ρ is the fluid density and μ is the dynamic viscosity.

3.2 Choice of time step

For transient ship resistance computations ITTC proposes the formulae $\Delta t = 0.005 - 0.01L/U$, where L is the length of the ship between perpendiculars and U is the ship advance speed. The maximum time step should not exceed this value.

3.3 Simulation design

DTMB 5415 naval surface combatant model has been chosen for the investigation of turning and zig-zag maneuvering performance. The ship includes both a sonar dome and a transom stern. The model is un-appended except for port and starboard bilge keels, i.e., not equipped with shaft, struts, propellers, or rudders for static drift simulations. To obtain rudder coefficients, twin rudders then implemented to the geometry and rudder drift simulations have been carried out. The model scale ratio is $\lambda=46.588$, which is DTMB 5512 in literature. The principal particulars of the ship are given in Table 1. The 3-D view of the ship model with a sonar dome and a transom stern including bilge keels is represented in Fig. 2.

Standard PMM tests consist of both static and dynamic captive model tests (Gertler 1967). To predict the maneuvering characteristics of the naval surface combatant, a series of static drift tests, e.g., static drift and drift and rudder, have been simulated using a commercial RANS solver.

The hull is considered as fixed during the simulations as in the experiment (Yoon 2009). In static drift simulations, drift angle is changed from 0 to 20 degrees. Similarly, in static rudder tests, rudder angle is switched from 0 to 35 degrees but drift angle is fixed at 0 degree (Simonsen *et al.* 2012). Drift and rudder tests are composed of static drift and static rudder tests, i.e., drift and rudder angles are changed parametrically (Table 2). Hydrodynamic analyses have been carried out for a fixed Froude number.



Fig. 2 3-D view of DTMB 5415 (Duman 2016)

Table 1 Principal particulars of DTMB 5415 (SIMMAN 2014)

	Model	Ship
λ	46.588	-
L_{BP} (m)	3.048	142
L_{WL} (m)	3.052	142.18
B_{WL} (m)	0.409	19.06
B_M (m)	0.429	20
T_M (m)	0.132	6.15
S (m ²)	1.37	2972.6
∇ (m ³)	0.084	8424.4
C_B	0.507	0.507
C_M	0.821	0.821
Fn	0.28	0.28

Table 2 Numerical simulation cases

Static drift		Static rudder		Drift and rudder	
Drift angle (°)	Rudder angle (°)	Drift angle (°)	Rudder angle (°)	Drift angle (°)	Rudder angle (°)
0	0	0	0	0	0, 5, 10, ..., 30, 35
2	0	0	5	4	0, 5, 10, ..., 30, 35
4	0	0	10	8	0, 5, 10, ..., 30, 35
6	0	0	15	12	0, 5, 10, ..., 30, 35
9	0	0	20	16	0, 5, 10, ..., 30, 35
10	0	0	25	-	-
11	0	0	30	-	-
12	0	0	35	-	-
16	0	-	-	-	-
20	0	-	-	-	-

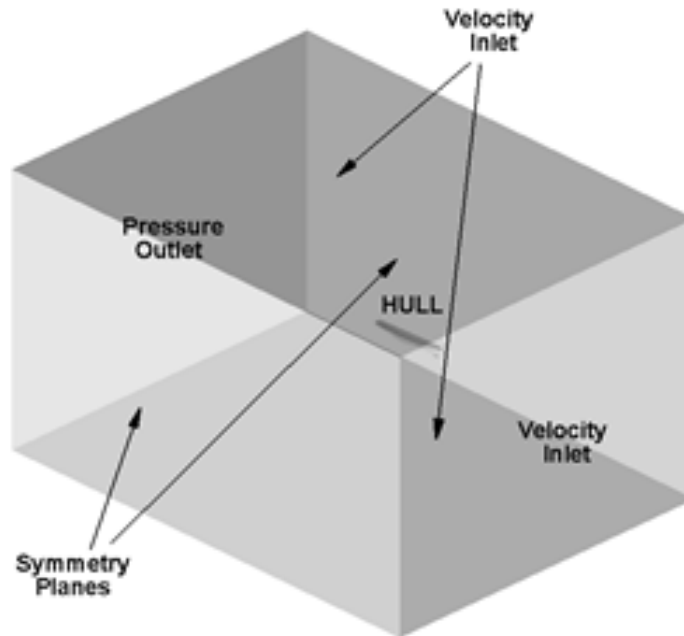


Fig. 3 Computational domain and boundaries

The computational domain and boundary conditions are illustrated in Fig. 3. The origin of the coordinate system is the intersection point of forward perpendicular and base line. Ship boundaries are identified as no slip walls where the normal and tangential components of the velocity are to be zero. Front, top and bottom faces of the computational domain are defined as velocity inlets. Side faces are assigned as symmetry-planes and the back face is defined as pressure outlet. Symmetry type of boundary condition enables to reduce the computational domain size and mesh number by half. In order to calculate the free surface deformations at the interaction of two phases (air and water) VOF method, the free surface is defined as calm water initially.

The computational domain dimensions are given in Table 3. Upstream is in the negative and downstream is in the positive x-direction. The top boundary indicates the distance between top of domain and the origin of the coordinate system. The bottom boundary is assigned in the same way. The computational domain is generated by considering the recommendations (ITTC 2011 and Tezdogan *et al.* 2015) and the previous experiences to be adequate in dimensions to simulate the flow around the ship hull properly.

Table 3 Computational domain dimensions (Duman 2016)

		Domain dimensions
Boundaries	Upstream	$1.8L_{BP}$
	Downstream	$3.6L_{BP}$
	Top	$1.6L_{BP}$
	Bottom	$2.1L_{BP}$
	Transverse	$2.4L_{BP}$

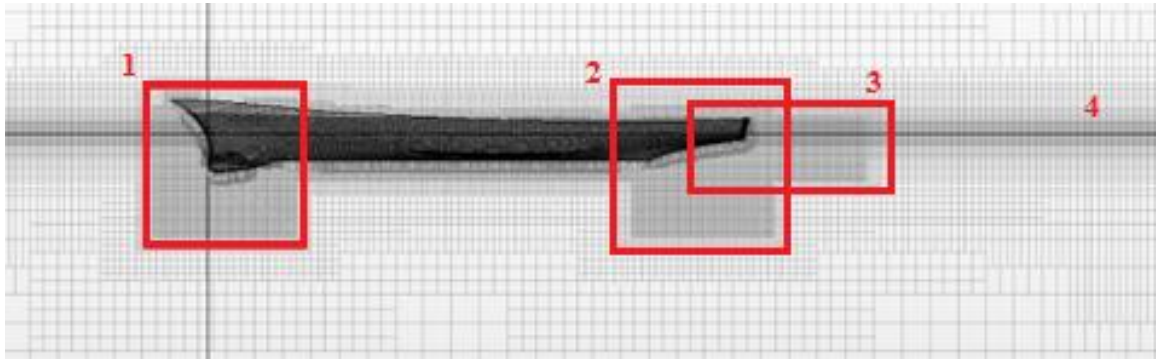


Fig. 4 Mesh refinements near the hull and the free surface

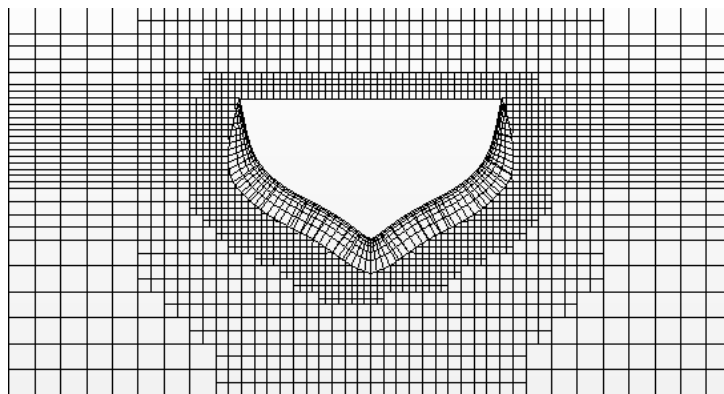


Fig. 5 Grid topology: $x/L=0.8$

Finite volume method is applied to discretize the computational domain. Fully unstructured hexahedral elements are used in order to generate the computational grid. Local volumetric controls have been used to refine the grid around the hull, bow and stern, free surface and wake zone.

Numbers 1 and 2 in Fig. 4 represent the bow and stern mesh refinements. In the wake zone of the hull, a cylindrical volumetric control represented with number 3 is generated to capture the free surface deformations. Number 4 indicates the free surface mesh refinement to capture the Kelvin waves properly. Grid structure of a section plane at $x/L=0.8$ is given in Fig. 5.

There are two geometries that can be used to refine the mesh around the free surface. These are rectangular and triangular volumetric controls (Fig. 6). The main idea of using triangular volumetric controls is to reduce the computational costs. Since the Kelvin waves have a specific spreading angle ($19^{\circ} 28'$), it makes sense to transform the rectangular refinements into triangular ones. A study has been made to compare the effects of triangular and rectangular mesh refinements around the free surface. It is seen that triangular mesh refinements give almost the same results as the rectangular ones. Considering the computational capability, triangular mesh refinements are preferred for the simulations (Fig. 6(a)).

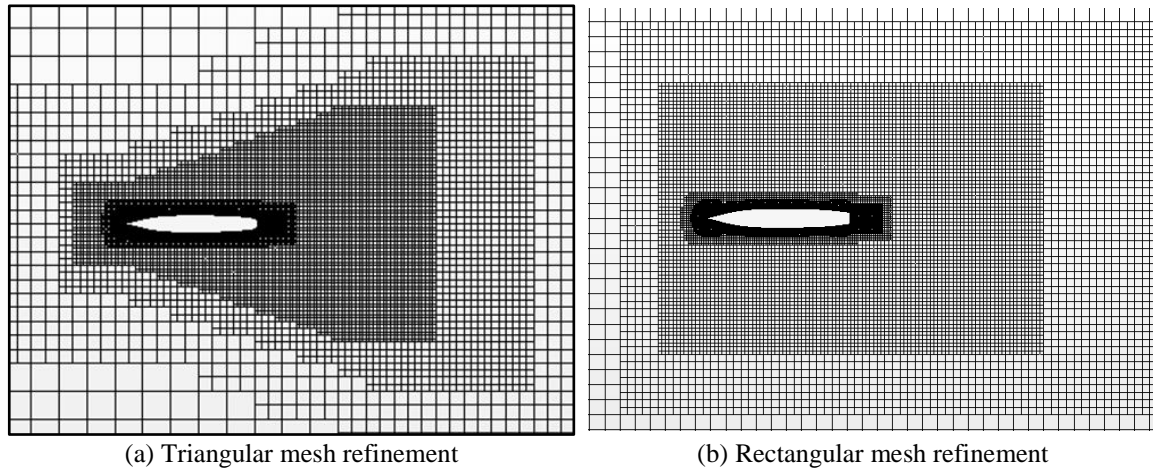


Fig. 6 Triangular and rectangular volumetric controls around the free surface

4. Computational results

It is crucial to compare the CFD simulation results with experiments. First, the grid independence study has been carried out. The effects of turbulence model have then been investigated and a comparison of viscous and inviscid models has been done. Validation of the hydrodynamic forces and moments, free surface deformations, hydrodynamic (manoeuvring) derivatives and a fast-time manoeuvring simulation results are presented, respectively.

4.1 Grid independence study

The grid sensitivity analyses have been made by Grid Convergence Method, which was firstly proposed by (Roache 1994) for $\beta=10^\circ$ drift angle. Static drift simulations have been repeated for three different grid qualities. The coarse grid is generated by multiplying base size of medium grid by the square root of two and the fine grid is generated by dividing base size of medium grid by the square root of two. Note that the total number of cells does not take a value of the multiplication or division of two-root-two due to the mesh algorithm used in the computations. Therefore, the refinement factors were calculated by considering the total cell numbers (Eq. (9)).

$$r_{21} = \left(\frac{N_2}{N_1} \right)^{1/3} \quad r_{32} = \left(\frac{N_3}{N_2} \right)^{1/3} \quad (9)$$

where N_1 , N_2 and N_3 are total cell numbers and $N_1 < N_2 < N_3$. The difference between any scalar results of the simulations of two different grids can be calculated as follows

$$\varepsilon_{21} = X_2 - X_1 \quad \varepsilon_{32} = X_3 - X_2 \quad (10)$$

As a scalar result, the sway forces acting on the hull have been chosen in this verification study. Convergence condition R can be calculated by the ratio of ε values (Eq. (11)). Details about the

uncertainty assessment can be found in (Celik *et al.* 2008).

$$R = \frac{\epsilon_{21}}{\epsilon_{32}} \tag{11}$$

The convergence conditions can be listed as follows

$$\begin{aligned} -1 < R < 0 & \quad \text{Oscillatory convergence} \\ 0 < R < 1 & \quad \text{Monotonic convergence} \\ R < -1 & \quad \text{Oscillatory divergence} \\ R > 1 & \quad \text{Monotonic divergence} \end{aligned} \tag{12}$$

In this study, the convergence condition was calculated as 0.477, which means the numerical results converge to a certain value as the grid becomes finer. Moreover, closer results to measurements can be obtained by increasing the number of cells. The behaviour of the convergence is monotonic (Eq. (12)). The uncertainty in the computations was calculated as 1.54%. Grid topologies of different grid qualities are given in Figs. 7(a)-7(f).

The numerical results of different grid qualities have been compared with the available experimental data. The relative errors between the numerical and the experimental results are given in Table 4. The experimental results are provided by IIHR where the static and dynamic manoeuvring experiments were carried out for three different Froude numbers. Details about the captive manoeuvring tests can be obtained from Yoon (2009) and Yoon (2015).

Since the relative difference between fine and medium grid results is about 1.48%, medium grid (Figs. 7(c) and 7(d)) has been used in the simulations in order to reduce the computational cost. The computation times are given in Table 5 for each grid quality. A workstation with 18 processors and 64 gb RAM (Random Access Memory) have been used for the computations.

Since the simulation results have quasi-steady characteristics after about 20 seconds, the total solution time is set as 100 seconds for all simulations and the time averages have been taken to obtained mean values of scalars in the quasi-steady interval, e.g., surge and sway forces. As an example, total resistance graph from the numerical results for $\beta=0^\circ$ and $\delta=0^\circ$ condition is given in Fig. 8.

Table 4 Numerical results of different grid qualities

Grid quality	Cell number	X'	Y'	% ϵ_X	% ϵ_Y
Fine	2,363,291	0.02016	0.06092	3.13	4.66
Medium	1,124,926	0.02050	0.06002	4.85	6.07
Coarse	568,844	0.02082	0.05813	6.52	9.03

Table 5 Numerical results of different grid qualities

Grid quality	Cell number	Computation time (hour)
Fine	2,363,291	38.5 h
Medium	1,124,926	20.8 h
Coarse	568,844	10 h

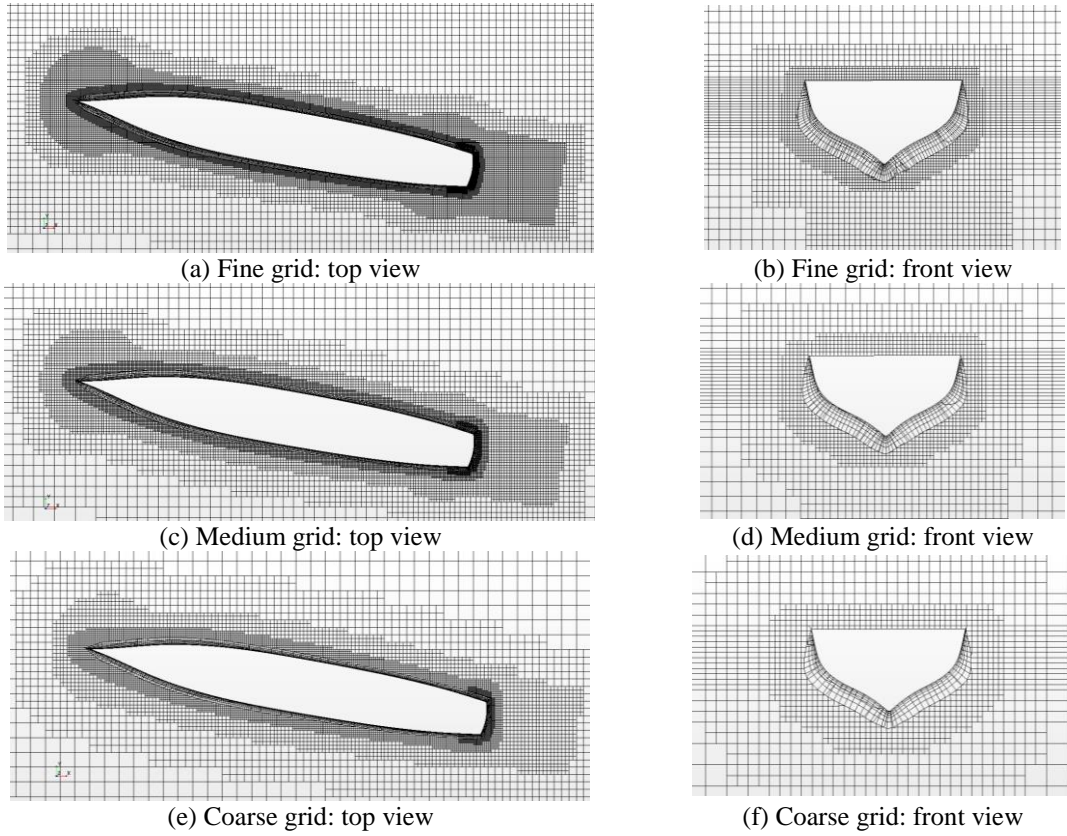


Fig. 7 Grid topologies of different cell numbers

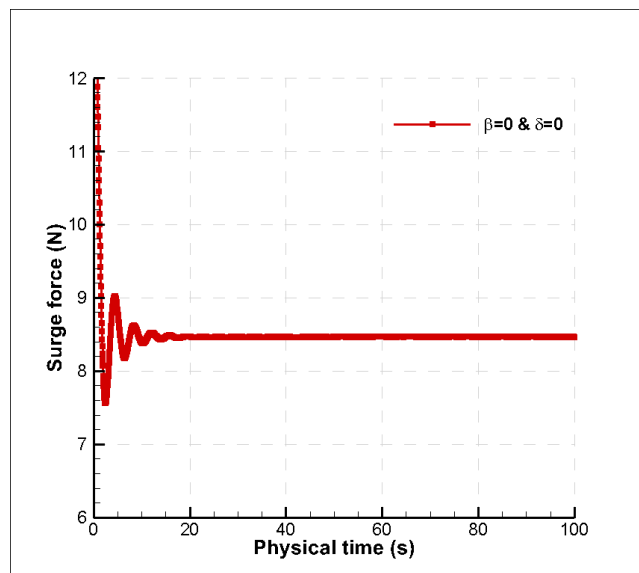
Fig. 8 Total resistance graph from the $\beta=0^\circ$ and $\delta=0^\circ$ CFD simulation

Table 6 Numerical results for two-equation models

Static drift	Turbulence model	X'	Y'	N'	% ε_X	% ε_Y	% ε_N
$\beta=2^\circ$	$k-\omega$ SST	0.01870	0.01117	0.00515	15.77	26.26	11.89
$\beta=2^\circ$	$k-\varepsilon$	0.01822	0.01134	0.00513	12.84	28.13	11.57
$\beta=12^\circ$	$k-\omega$ SST	0.02251	0.07049	0.02706	12.28	2.30	17.62
$\beta=12^\circ$	$k-\varepsilon$	0.02163	0.07159	0.02713	7.90	0.77	17.42

4.2 The effects of turbulence model

The effects of turbulence model have been investigated for $\beta=2^\circ$ and $\beta=12^\circ$ static drift angles. The results ($k-\omega$ and $k-\varepsilon$) are compared with each other and also with the EFD data (Table 6).

Surge forces and yaw moment are calculated satisfactorily by using $k-\varepsilon$. Although, $k-\omega$ SST gives better results in the calculation of sway forces at low drift angles, $k-\varepsilon$ turbulence model gives more accurate results than $k-\omega$ SST for the overall table. Therefore, $k-\varepsilon$ turbulence model is used for the following hydrodynamic analyses.

4.3 Comparison of viscous and inviscid models

Viscosity has a significant role in predicting ship maneuvering performance. A study has been conducted by Duman and Bal (2016) to investigate the viscous effects on static drift tests. The viscous model results have been compared with those of inviscid cases, via forces and moments acting on the hull (Table 7).

It is seen that the inviscid model is not sufficient to estimate surge forces since there is no frictional resistance in the longitudinal direction. It should be noted that surge forces occur due to wave-induced force here. As the drift angle increases, the wave resistance in surge direction also increases due to larger frontal area. Thus, surge forces get closer to the viscous results.

Table 7 Numerical results of viscous and inviscid models

Drift angle ($^\circ$)	Viscous model results			Inviscid model results			Deviations		
	X'	Y'	N'	X'	Y'	N'	s_X'	s_Y'	s_N'
0	0.01722	0.00000	0.00000	0.00658	0.00000	0.00000	161.71	-	-
2	0.01726	0.01124	0.00517	0.00687	0.00896	0.00511	151.14	25.47	1.31
6	0.01812	0.03211	0.01566	0.00768	0.02732	0.01532	135.86	17.52	2.23
9	0.01934	0.04688	0.02400	0.00904	0.04130	0.02346	113.83	13.49	2.31
10	0.02001	0.05183	0.02664	0.01021	0.04655	0.02577	96.05	11.35	3.38
11	0.02043	0.05754	0.02902	0.01094	0.05268	0.02847	86.71	9.23	1.95
12	0.02122	0.06303	0.03106	0.01234	0.05885	0.03066	72.03	7.10	1.28
16	0.02611	0.09372	0.03881	0.01939	0.08671	0.03779	34.65	8.09	2.70
20	0.03244	0.13059	0.04650	0.02438	0.11561	0.05044	33.07	12.96	7.81

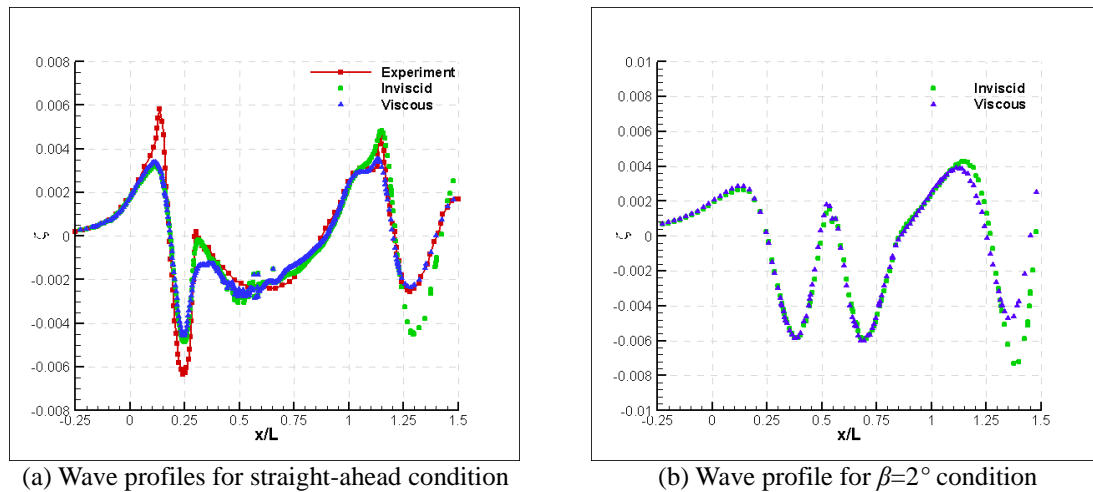


Fig. 9 Comparison of viscous and inviscid models

Sway forces and yaw moment from inviscid model seem to be close to viscous results. This can be explained by the fact that the wave making resistance is dominant at Froude number 0.28. The wave deformations for straight-ahead and $\beta=2^\circ$ condition are given in Fig. 9. The wave profiles from viscous and inviscid models are close to each other especially in the bow region. However, in the wake zone inviscid wave amplitudes are larger than viscous ones, since there is no damping caused by the viscosity.

4.4 Validation of forces and moments

Forces and moments acting on the gravity centre of the hull have been calculated for each case. The mean values of these quantities are obtained from time-averages of numerical results. The averaging operations are performed within the quasi-steady state interval. The un-appended simulation results are compared with experiments in Table 8 and presented in Fig. 10. The experiments are performed in a 3.048x3.048x100 m towing tank. Fixed and free to sinkage and trim conditions have been performed. The forces/moment and uncertainty analysis (UA) are conducted in collaboration with two international facilities (FORCE and INSEAN). Hydrodynamic derivatives are determined from the forces/moment data by using the Abkowitz (1966) mathematical model, with two different “Multiple-Run (MR)” and “Single-Run” methods. Detailed information about the experiments is available in the doctoral dissertation of Yoon (2009). Forces and moments are given in the ship-fixed coordinate system. X' , Y' and N' indicate the non-dimensional surge force (resistance), sway force and yaw moment, respectively.

As seen in Table 8, computational results are agreeable with experiments. It is observed that the percentage of error decreases with the increase of drift angle for sway forces where drift angle is less than 9° . However, yaw moment increases significantly for drift angles higher than 11° .

Fig. 10 shows that surge forces obtained by CFD are slightly higher than the experiments. Sway forces show good agreement especially for drift angles lower than 11° . Computational analyses of appended hull have also been performed to include the rudder effects. The additional forces and moments acting on the hull due to the rudders are given in Table 10.

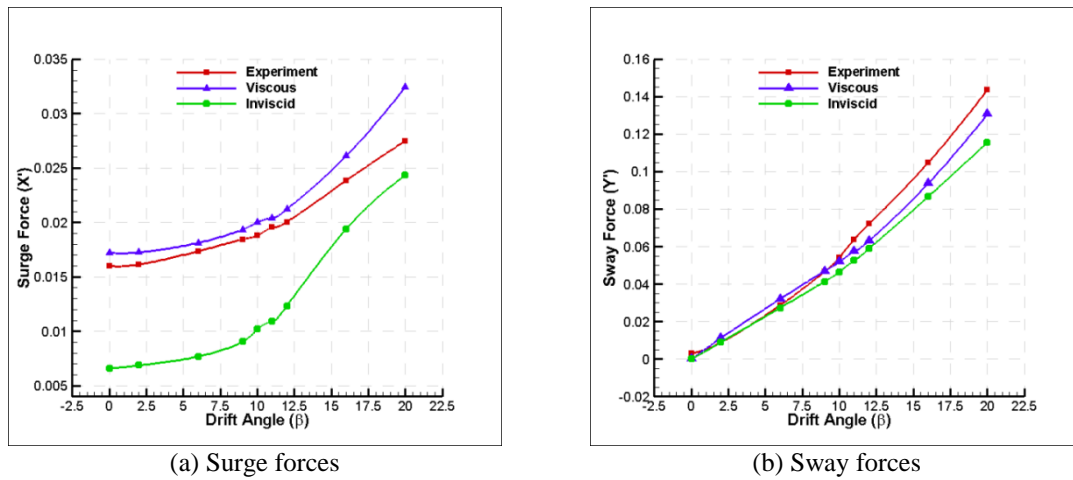


Fig. 10 Comparison of CFD and experiments for un-appended model via forces

Table 8 Validation of numerical results for un-appended model

Drift angle (°)	X'	Y'	N'	X _{EFD} '	Y _{EFD} '	N _{EFD} '	% ε _X	% ε _Y	% ε _N
0	0.01722	0.00000	0.00000	0.01600	0.00320	0.00100	7.62	-	-
2	0.01726	0.01124	0.00517	0.01615	0.00885	0.00460	6.85	26.97	12.48
6	0.01812	0.03211	0.01566	0.01735	0.02870	0.01500	4.43	11.87	4.41
9	0.01934	0.04688	0.02400	0.01845	0.04670	0.02310	4.81	0.38	3.89
10	0.02001	0.05183	0.02664	0.01880	0.05430	0.02620	6.42	4.55	1.68
11	0.02043	0.05754	0.02902	0.01955	0.06390	0.03000	4.48	9.96	3.26
12	0.02122	0.06303	0.03106	0.02005	0.07215	0.03285	5.86	12.64	5.46
16	0.02611	0.09372	0.03881	0.02385	0.10485	0.04490	9.46	10.61	13.56
20	0.03244	0.13059	0.04650	0.02750	0.14365	0.05530	17.96	9.09	15.91

The rudders have several effects on the numerical results. In the presence of the twin-rudder at neutral position ($\delta=0^\circ$), surge forces decrease with the increase of drift angles. However, yaw moments decrease due to the torque generated by the rudders in the opposite direction with the one generated by the hull.

The sway forces on the other hand increase due to the extra forces generated by the rudders in the same direction with the sway forces by the hull. The wave deformations along the hull are similar to each other except that there is a slight decrease in the wake zone when the rudders are placed behind the hull (Fig. 11(b)). The flow around the rudders might have generated low pressure field that could pull down the free surface. The changes in forces and moment are given in Table 9 and shown in Fig. 11.

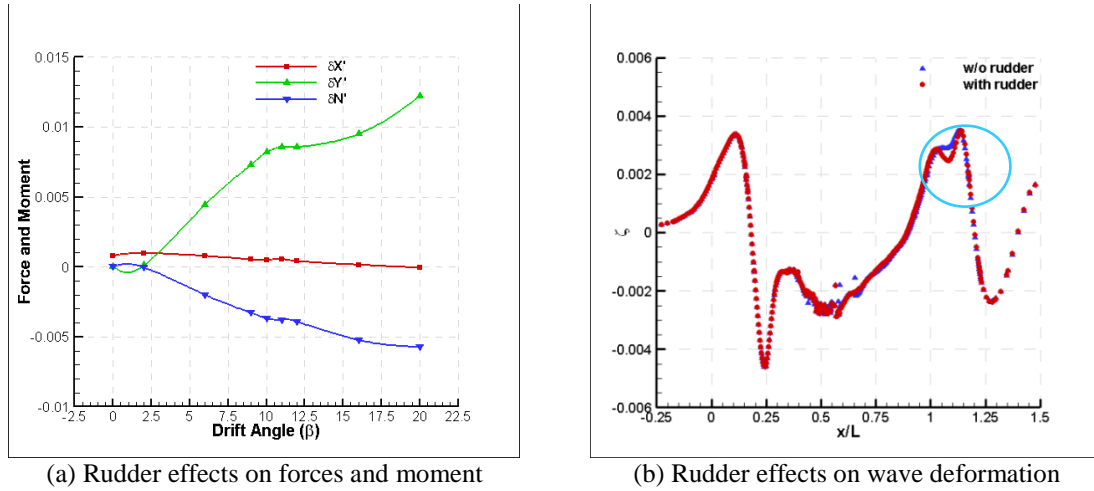


Fig. 11 The rudder effects on the numerical results

Table 9 Additional forces and moments due to the rudders

Drift angle (°)	$\Delta X'$	$\Delta Y'$	$\Delta N'$
0	0.00079	0.00000	0.00000
2	0.00097	0.00010	-0.00004
6	0.00077	0.00444	-0.00201
9	0.00052	0.00730	-0.00329
10	0.00049	0.00819	-0.00369
11	0.00055	0.00858	-0.00381
12	0.00041	0.00856	-0.00393
16	0.00014	0.00950	-0.00524
20	-0.00006	0.01220	-0.00574

4.5 Free surface deformations

As it is known, nonlinearities and flow separation increase at high drift angles. The free surface deformations for $\beta=0^\circ$ and $\beta=20^\circ$ (static drift cases) have been investigated and compared with the available experimental data. The first case is straight-ahead condition. The free surface wave contours are presented in Fig. 12(a). The free surface deformations obtained from numerical analyses are compared with the experiments (Longo *et al.* 2005) in Fig. 12(b), where the x-axis is non-dimensional ship length and y-axis is non-dimensional transverse distance. The free surface

waves can clearly be seen that they are compatible with the experimental results. The free surface rises behind the sonar dome and a wave crest is also generated in the wake zone of the hull (Fig. 12(b)).

The next case is $\beta=20^\circ$ static drift condition. Free surface rise at the bow region of the hull and the flow is also separated at bow and aft, as shown in Fig. 13(b). A particular section is also taken from the free surface at $y/L=0.302$ on leeward side for $\beta=20^\circ$ condition. The location of this particular section can be seen in Fig. 13(d). The wave profile on this section is compared with the available data in Fig. 13(c). The trend of the wave profile on the leeward side is satisfactory with the experiments. The x-axis and y-axis of Fig. 13(b) are the non-dimensional x-position and wave elevation, respectively.

A wave trough around the first quarter and the last quarter of the ship can be seen in both figures. Three wave crests can also be noticed around the $x/L=0.6$, $x/L=0.85$ and $x/L=1.30$ positions. Fig. 13(a) illustrates the flow separation around sonar dome via vorticity magnitude scale.

4.6 Hydrodynamic derivatives

The forces and moments calculated from static drift simulations are used to determine the hydrodynamic derivatives. These derivatives are given in Table 10 and some of them are compared with the experimental data. Several empirical formulas are used to calculate the linear derivatives and compared with numerical and experimental results in Table 11 (Smitt 1970, Norrbin 1971, Inoue *et al.* 1981, Clarke and Gedling 1982, Ankudinov 1987).

4.7 Maneuvering simulation results

The straight-line stability index is first calculated as $C=0.00082$ (see in Table 12) which is bigger than zero and it means model has straight-line stability.

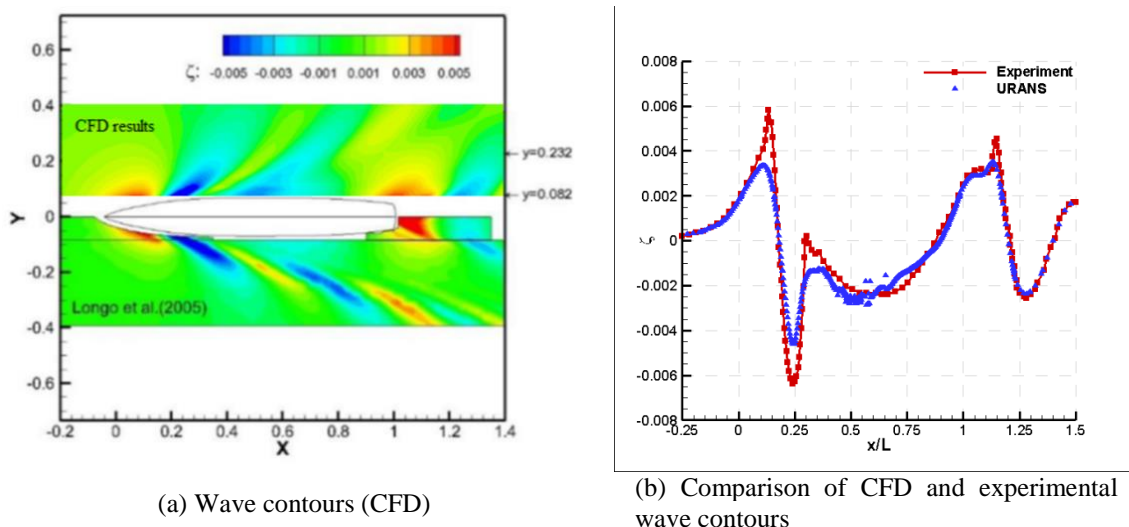
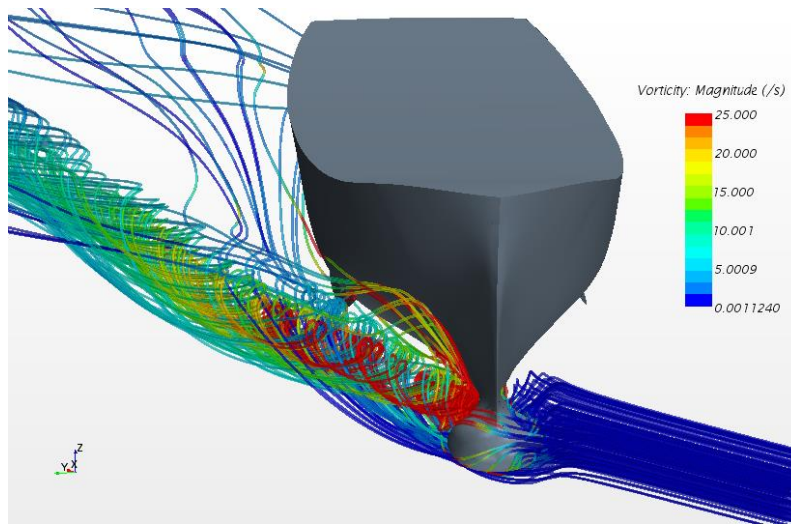
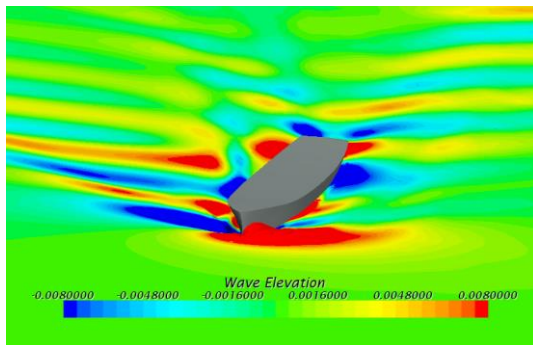


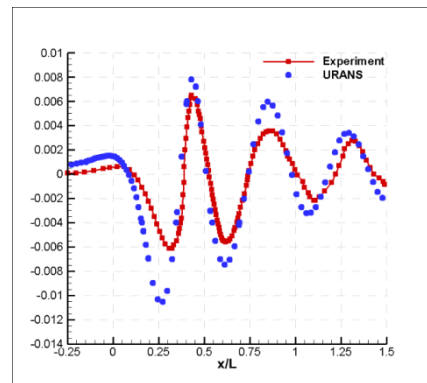
Fig. 12 Free surface deformations for straight-ahead condition



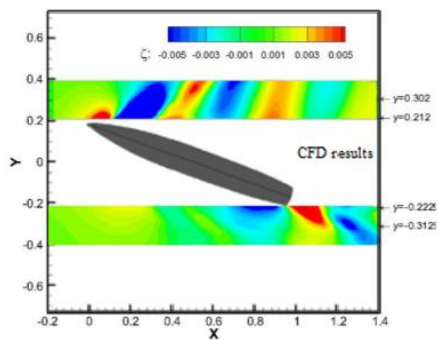
(a) Flow separation around the sonar dome



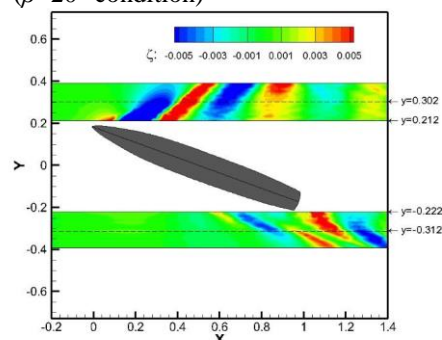
(b) Wave contours from perspective view (CFD)



(c) Wave profiles at $y/L=0.302$ on leeward side ($\beta=20^\circ$ condition)



(d) Wave contours for $\beta=20^\circ$ (CFD)



(e) Wave contours for $\beta=20^\circ$ (experiment)

Fig. 13 Free surface deformations for $\beta=20^\circ$ condition

A computer program has been developed to apply a fast simulation technique in MATLAB.

The rudder deflections, principal particulars of the model and hydrodynamic maneuvering coefficients have been used as inputs in the program. Euler method is used to solve the differential equations of ship maneuvering motion simultaneously. Abkowitz's non-linear model is adopted to calculate the forces and moment acting on the hull during maneuvering motion (Abkowitz 1964).

The time step is chosen as 1×10^{-2} (non-dimensional time). Since the linear and angular velocity terms are known for each time step, the yaw angle, drift angle, turning circle diameter, tactical diameter, advance and transfer distances are then calculated. Turning and zig-zag maneuvering simulations have been carried out and the maneuvering characteristics have been determined. The CFD simulation results and results of a fast maneuvering simulation have been compared with the available experimental data. The turning circle diameter is compared with the linear model and the empirical formulas. The tactical diameter is compared with the experiments.

Table 10 Hydrodynamic derivatives

Drift and rudder						Static drift			
Deriv.	Num. results	Deriv.	Num. results	Deriv.	Num. results	Deriv.	Num. results	(Yoon 2009)	% ϵ
X_δ'	-0.0205	Y_δ'	0.02975	N_δ'	0.1416	$X^{*'}_v$	-0.0185	-0.0170	8.82
$X_{\delta\delta}'$	0.0837	$Y_{\delta\delta\delta}'$	-0.0928	$N_{\delta\delta\delta}'$	-0.0303	X_{vv}'	-0.1688	-0.1528	10.47
$X_{v\delta}'$	-1.1106	$Y_{\delta v}'$	3.3048	$N_{\delta u}'$	4.9011	Y_v'	-0.3970	-0.2961	34.08
$X_{\delta\delta u}'$	10.0370	$Y_{\delta v v}'$	-12.2940	$N_{\delta\delta\delta u}'$	34.9550	Y_{vvv}'	-2.0947	-1.9456	7.66
		$Y_{v\delta\delta}'$	-6.7551	$N_{\delta v v}'$	-0.1985	N_v'	-0.1395	-0.1667	16.32
		$Y_{\delta u}'$	-3.7854	$N_{v\delta\delta}'$	13.9600	N_{vvv}'	-0.0777	-0.4355	82.16
		$Y_{\delta\delta\delta u}'$	-12.5000						

Table 11 Comparison of empirical, numerical and experimental results

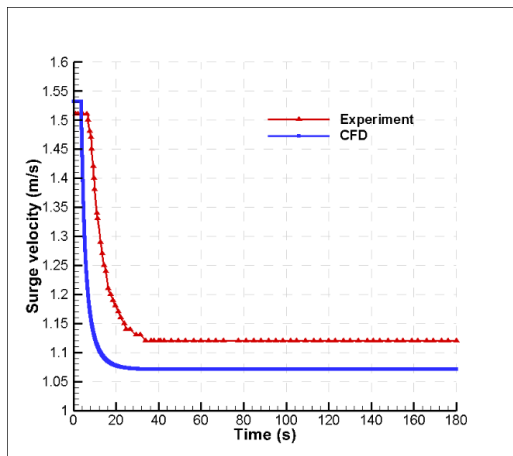
Derivative	Numerical results	Experiment	Norrbin	Clarke	Inoue	Wagner Smitt	Ankudinov
Y_v'	-0.3970	-0.2961	-0.0102	-0.0063	-0.0102	-0.0094	-0.0098
Y_r'	-	-0.0485	0.0026	0.0027	0.0029	0.0019	0.0000
N_v'	-0.1395	-0.1667	-0.0036	-0.0036	-0.0038	-0.0037	-0.0043
N_r'	-	-0.0485	-0.0022	0.0092	-0.0571	-0.0012	-0.0020

Table 12 Non-dimensional straight-line stability terms

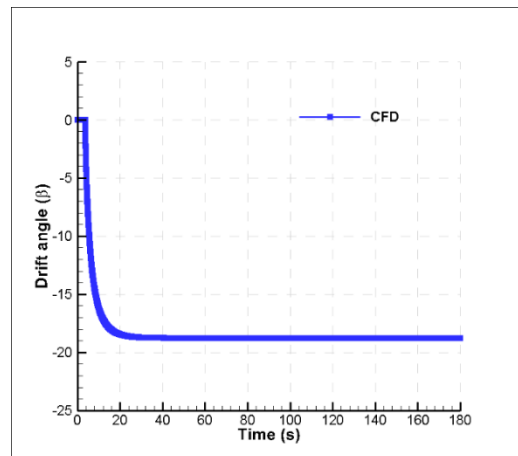
Stability index terms	m	x_g	Y_v	N_v	Y_r	N_r
Quantity	0.0058	0.5052	-0.3970	-0.1395	-0.1970	-0.0704
Stability index C	0.00082					

Table 13 Comparison of the turning maneuver parameters

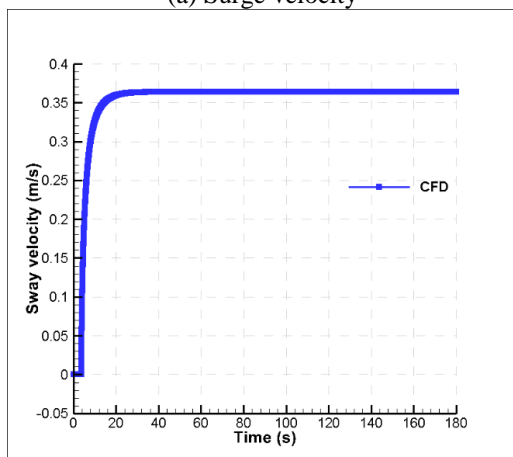
	Steady turning radius (m)		Tactical diameter (m)
Non-linear model	1.52L _{pp}	Fast-time simulation	3.19L _{pp}
Linear model	1.33L _{pp}	FORCE PMM	4.05L _{pp}
Thieme	0.26L _{pp}	SAIC_LAMP_PMM	4.2L _{pp}
Schoenherr	2.61L _{pp}	MARIN - FreeSim	4.59L _{pp}
Lyster & Knight	2.46L _{pp}	MARIN - SurSim	2.64L _{pp}
		MARIN - FreDyn (v9.9)	4.94L _{pp}
		IOWA RANS Cst RPM (CFD)	4.6L _{pp}



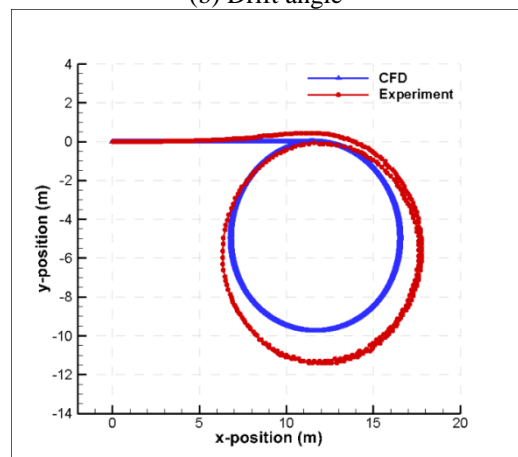
(a) Surge velocity



(b) Drift angle



(c) Sway velocity

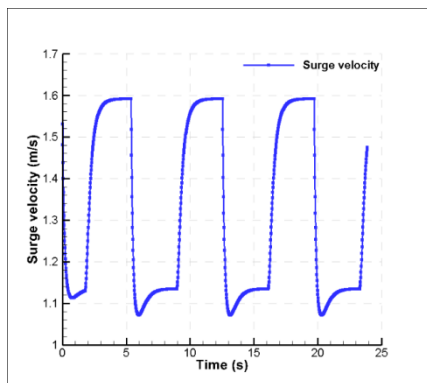


(d) Turning circle

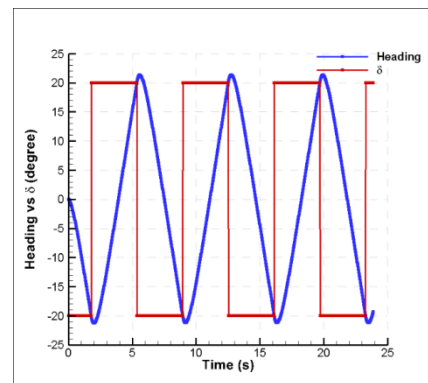
Fig. 14 Fast-time turning circle simulation results

Table 14 Comparison of the zig-zag maneuver parameters

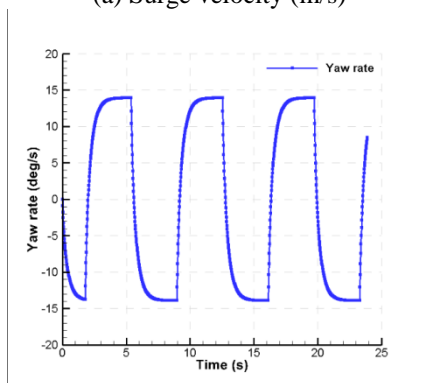
	Overshoot angles		
	10°/10° zig-zag		20°/20° zig-zag
	1 st Overshoot	2 nd Overshoot	1 st Overshoot
Statistics	3°	5°	6°
Fast-time simulation	1.48°	1.54°	1.25°
MARIN - SurSim	3.7°	5.2°	11.9°
MARIN - SurSim_sb	10.3°	28.7°	36.0°
MARIN - FreSim	2.9°	3.1°	7.0°
MARIN - FreSim_sb	5.3°	6.0°	12.0°
MARIN - MPP	7.3°	11.3°	13.7°
MARIN - FreDyn	1.7°	1.8°	4.5°



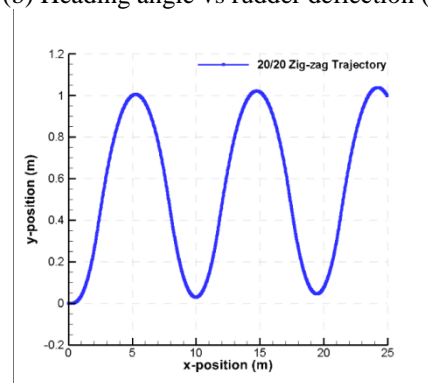
(a) Surge velocity (m/s)



(b) Heading angle vs rudder deflection (°)



(c) Yaw rate (deg/s)



(d) 20°/20° Zig-zag maneuvering trajectory

Fig. 15 Fast-time simulation results for 20°/20° zig-zag maneuver

The results of turning maneuver simulation of DTMB5415 hull are presented in Fig. 14. Surge velocity, yaw rate, sway velocity and drift angle converge to certain values, which means that the ship turns on a steady turning circle.

The steady turning radius can be calculated by using basic angular motion formulae. The norm of the velocity divided by yaw rate gives the steady turning radius. Trajectory of the ship is calculated by integrating the velocities over the solution time and plotted in Fig. 14(d), where the x-axis and y-axis are dimensional x and y positions in Earth-fixed coordinate system, respectively. The steady turning radius is presented with those of the linear model, non-linear model and several empirical formulas. The tactical diameter is also compared with the experimental and other numerical data (Table 13). The nonlinear model estimates the steady turning diameter higher than linear model. It should be noted that the empirical formulas were proposed for cargo ships and not suitable for warships.

The resultant turning maneuver trajectory is presented in Fig. 14(d) in comparison with the experimental results as given in Hajivand and Mousavizadegan (2015). The rudder angle during the turning maneuver is set to $\delta=35$ degree. Steady turning diameter of CFD is found to be lower than the experimentally determined one. Decrease in the model's resultant velocity during the steady turning maneuver is calculated as 0.26%. The computational errors due to choosing a medium grid may have caused the difference between CFD and experiments. Using finer grid and improving the local grid refinements around the hull may lead us to better results.

After turning circle simulations, zig-zag maneuvering performance of DTMB 5512 has been investigated by performing $10^\circ/10^\circ$ and $20^\circ/20^\circ$ zig-zag simulations. The first and second overshoot angles are primarily concerned in $10^\circ/10^\circ$ zig-zag test while the first overshoot angle is important in $20^\circ/20^\circ$ zig-zag test. Surge velocity, heading angle, yaw rate and $20^\circ/20^\circ$ zig-zag maneuvering trajectory are given in Fig. 15, respectively. Zig-zag maneuvering trajectory has been calculated by integrating the surge and sway velocities over the solution time. The heading angle versus rudder deflection are given in Fig. 15(b). The rudder angle has been switched directly from one side to another without any lag. Since the sway motion amplitude is smaller than surge motion, only the 25 m long from the start of the motion is represented in Fig. 15(d). The fast-time zig-zag simulation results are given in Table 14 in comparison with the available data in literature (Toxopeus *et al.* 2008). It is seen that the zig-zag maneuvering results are below the statistics. Further studies are necessary in order to reduce numerical errors in the calculation of hydrodynamic derivatives. The fast-time simulation code is also needed to be improved for more realistic cases.

5. Conclusions

The nature of ship maneuvering problems is highly complex and nonlinear. The assessment of ship-maneuvering performance in the early design stage has a significant role to get a sufficient adequacy of ship's controllability. Turning and zig-zag maneuvering characteristics of the US Navy surface combatant DDG51 guided missile destroyer in 1/46.588 model scale ratio have been investigated by performing URANS computations and fast-time maneuvering simulations. First, the numerical method has been validated for un-appended model by performing static drift simulations. After validation of the method, rudders have been implemented to the model in order to calculate the rudder coefficients. The angular velocity, acceleration and cross-coupled terms have been taken from the available experimental data. A computer program has been developed in

order to apply a fast-time simulation technique. Abkowitz's nonlinear mathematical method is adopted to calculate the forces and moment acting on the hull during the maneuvering motion. Euler method has been used to solve simultaneous differential equations of ship maneuvering motion.

The meshing algorithm that has been constructed in this study makes it possible to solve the flow around the hull with lower mesh numbers. Specific conditions have been investigated with two different turbulence models ($k-\varepsilon$ and $k-\omega$ SST) in order to determine the appropriate model for hydrodynamic analyses. Although, $k-\omega$ SST turbulence model gives better results in the calculation of sway force at low drift angles, $k-\varepsilon$ turbulence model gives more accurate results than $k-\omega$ SST for all other cases given in this paper. Therefore, $k-\varepsilon$ turbulence model has been used for the hydrodynamic analyses. The computational results show good agreement with the experiments. It is found that reasonably accurate results have been obtained by URANS method. It is also found that the wave profiles along the ship model are in a good agreement with the experiments both at straight-ahead and at high drift angle conditions. The viscous effects have been investigated for un-appended hull at all static drift cases by applying URANS and Eulerian (inviscid) approaches.

The inviscid results are found to be insufficient for capturing the wave deformations especially in the wake zone of the model.

The rudder terms have been calculated from the numerical simulations of appended hull. Turning and zig-zag manoeuvres of 5512 have been simulated by the fast-time simulation computer code and performance characteristics are determined. The turning manoeuvre performance parameters are compared with those of empirical formulas and available validation data and the results are promising. The first and second overshoot angles for $10^\circ/10^\circ$ and the first overshoot angle for $20^\circ/20^\circ$ are compared with the available data. The overshoot angles are calculated lower than the statistics. Further studies are needed in order to reduce the numerical errors in the calculation of hydrodynamic derivatives by improving the mesh quality. Virtual simulation of captive model tests and the calculation of the maneuvering coefficients can be used as a compact solution for determining the maneuvering performance of a vessel in the preliminary design stage.

In future work, dynamic manoeuvres will be simulated as well as the static manoeuvres by using overset grid technique and the acceleration, angular velocity and cross-coupled terms will be determined. The heel effects on the turning manoeuvre will be taken into account. The computational grid quality will also be increased. In addition to captive model tests, free-running tests will be simulated with CFD by using overset grid technique. The fast-time simulation program will be developed in order to simulate more realistic conditions, i.e., including the external forces and/or propulsion control etc.

References

- Abkowitz, M.A. (1964), Lectures on Ship Hydrodynamics – Steering and Maneuvering, Hy-5. Lyngby, Denmark: Hydro & Aerodynamic Laboratory.
- Ankudinov, V. (1987), "Ship maneuverability assessment in ship design", *International Ship Manoeuvring Conference*. London.
- Bal, S. (2008), "Prediction of wave pattern and wave resistance of surface piercing bodies by a boundary element method", *Int. J. Numer. Meth. Fl.*, **5**(3), 305-329.
- Bal, S. (2016), "Free surface effects on 2-D airfoils and 3-D wings moving over water", *Ocean Syst. Eng.*, **6**(3), 245-264.

- Bhushan, S., Xing, T., Carrica, P. and Stern, F. (2007), "Model- and full-scale URANS/DES simulations for athena R/V resistance, powering, and motions", *Numer. Ship Hydrodynam. Conference II*, 122-142.
- Celik, I., Ghia, U., Roache, P.J. and Christopher, J.F. (2008), "Procedure for estimation and reporting of uncertainty due to discretization in CFD applications", *J. Fluid. Eng.*, **130**(7), 1-4.
- Clarke, D.B. and Gedling, P. (1982), "The application of manoeuvring criteria in hull design using linear theory", *Transactions of the Institution of Naval Architects, RINA*.
- Duman, S. (2016), "Investigation of the turning performance of a surface combatant with URANS", Master's Thesis, Istanbul Technical University.
- Duman, S. and Bal, S. (2016a), "Numerical investigation of viscous effects on the static PMM tests of ships", *Proceedings of the 2nd International Meeting on Recent Advances in Prediction Techniques for Safe Manoeuvring of Ships and Submarines*. Istanbul, Turkey.
- Duman, S. and Bal, S. (2016b), "Numerical investigation of scale effects on maneuvering coefficients of DTMB 5415 hull", *Proceedings of the 1st International Congress on Ship and Marine Technology*, Piri Reis University, Tuzla, Istanbul, Turkey: The Chamber of Turkish Naval Architects and Marine Engineers.
- Ferziger, J.H. and Perić, M. (2002), *Computational Methods for Fluid Dynamics*, (3 Ed.), Berlin: Springer.
- Fossen, T.I. (1994), *Guidance and Control of Ocean Vehicles*, Chichester, New York: Wiley.
- Gertler, M. (1967), "The DTMB planar-motion-mechanism system", Test and Evaluation Report AD659053. Washington, DC: Naval Ship Research and Development Center.
- Hajivand, A. and Mousavizadegan, S.H. (2015), "Virtual simulation of maneuvering captive tests for a surface vessel", *Int. J. Naval Architect. Ocean Eng.*, **7**(5), 848-872.
- Hirt, C.W. and Nichols, B.D. (1981), "Volume of Fluid (VOF) method for the dynamics of free boundaries", *J. Comput. Phys.*, **39**(1), 201-225.
- Inoue, S., Hirano, M. and Kijima, K. (1981), "Hydrodynamic derivatives on ship manoeuvring", *Int. Shipbuild. Progress* **28**(321), 112-125.
- ITTC. (2011), "Practical guidelines for ship CFD applications", *Proceedings of the 26th ITTC*. In . Hague.
- Kim, H., Akimoto, H. and Islam, H. (2015), "Estimation of the hydrodynamic derivatives by RANS simulation of planar motion mechanism test", *Ocean Eng.*, **108**, 129-139.
- Kim, W.J., Van, S.H. and Kim, D.H. (2001), "Measurement of flows around commercial ship models", *Exp. Fluids*, **31**(5), 567-578.
- Kinaci, O.K., Sukas, O.F. and Bal, S. (2016), "Prediction of wave resistance by a reynolds-averaged navier-stokes equation-based computational fluid dynamics approach", *Proceedings of the Institution of Mechanical Engineers, Part M: Journal of Engineering for the Maritime Environment*, **230**(3), 531-548.
- Larsson, L., Stern, F. and Bertram, V. (2003), "Benchmarking of computational fluid dynamics for ship flows: The Gothenburg 2000 workshop", *J. Ship Res.*, **47**(1), 63-81.
- Longo, J. and Stern, F. (2005), "Uncertainty assessment for towing tank tests with example for surface combatant DTMB model 5415", *J. Ship Res.*, **49**(1), 55-68.
- Nikolaev, E. and Lebedeva, M. (1980), "On the nature of scale effects in manoeuvring tests with full-bodied ship models", *Proceedings of the 13th Symposium on Naval Hydrodynamics*, Tokyo, Japan.
- "Nomenclature for Treating the Motion of a Submerged Body through a Fluid" (1952), Technical and Research Bulletin 1-5. SNAME.
- Norrbin, N.H. (1971), "Theory and observations of on the use of a mathematical model for ship manoeuvring in deep and confined waters", *SSPA, Gothenburg, Sweden* 68.
- Roache, P.J. (1994), "Perspective: A method for uniform reporting of grid refinement studies", *J. Fluid. Eng.*, **116**(3), 405.
- Sakamoto, N. (2009), "URANS and DES simulations of static and dynamic maneuvering for surface combatant", PhD Thesis, University of Iowa.
- SIMMAN. (2014), "Geometry and conditions of US navy combatant", *simman2014.dk*. <http://simman2014.dk/ship-data/us-navy-combatant/geometry-and-conditions-us-navy-combatant/>.
- Simonsen, C.D., Otzen, J.F., Klimt, C., Larsen, N.L. and Stern F. (2012), "Maneuvering Predictions in the Early Design Phase Using CFD Generated PMM Data", *Proceedings of the 29th Symposium on Naval Hydrodynamics*, Gothenburg, Sweden.

- Simonsen, C.D. and Stern, F. (2003), "Verification and validation of RANS maneuvering simulation of Esso Osaka: Effects of drift and rudder angle on forces and moments", *Comput. Fluids*, **32**(10), 1325-1356.
- Smitt, W.L. (1970), "Steering and manoeuvring full-scale and model tests (Part 1)", *European Shipbuild.*, **19** (6).
- Stern, F., Wilson, R.V., Coleman, H.W. and Paterson, E.G. (2001), "Comprehensive approach to verification and validation of CFD simulations—Part 1: Methodology and procedures", *J. Fluid. Eng. -T ASME*, **123** (4), 793.
- Tezdogan, T., Demirel, Y.K., Kellett, P., Khorasanchi, M., Incecik, A. and Turan, O. (2015), "Full-scale unsteady RANS CFD simulations of ship behaviour and performance in head seas due to slow steaming", *Ocean Eng.*, **97**, 186-206.
- Uslu, Y. and Bal, S. (2008), "Numerical prediction of wave drag of 2-D and 3-D bodies under or on a free surface", *Turkish J. Eng. Environ. Sci.*, **32**, 177-188.
- Toxopeus, S. and Lee, S.W. (2008), "Workshop on Verification and Validation of Ship Manoeuvring Simulation Methods", *Proceedings of SIMMAN 2008 Workshop*.
- Yoon, H. (2009), "Phase-averaged stereo-PIV flow field and force/ moment/motion measurements for surface combatant in PMM maneuvers", PhD Thesis, University of Iowa.
- Yoon, H., Simonsen, C.D., Benedetti, L., Longo, J., Toda, Y. and Stern, F. (2015), "Benchmark CFD validation data for surface combatant 5415 in PMM maneuvers – Part I: force/moment/motion measurements", *Ocean Eng.*, **109**, 705-734.
- Yoshimura, Y. (2005), "Mathematical model for manoeuvring ship motion (MMG Model)", *Proceedings of the Workshop of Mathematical Models for Operations Involving Ship-Ship Interaction*, Tokyo, Japan.

Nomenclature

- x_G : Longitudinal center of gravity
 y_G : Transverse center of gravity
 z_G : Vertical center of gravity
 x, u : Surge motion, surge velocity
 y, v : Sway motion, sway velocity
 ε : Relative error
 z : Heave motion
 β : Drift angle
 φ : Roll motion
 θ : Pitch motion
 $\psi, \dot{\psi}$: Yaw motion, yaw rate (usually represented by “r”)
 ρ : Fluid density
 λ : Model scale ratio
 $\rho \bar{u}_i \bar{u}_j$: Reynolds stress
 Δt : Time step
 Δu : Perturbation in surge velocity
 C : Stability index
 CMT : Captive Model Tests
 DOF : Degree-of-freedom
 Fn : Froude number
 VOF : Volume of fluid
 I_x : Moment of inertia at x-axis
 I_y : Moment of inertia at y-axis
 I_z : Moment of inertia at z-axis
 L : Length of the ship
 N : Yaw moment acting on the gravity center of the hull
 N_v : Rate of change of yaw moment with sway velocity
 N_δ : Rate of change of yaw moment with rudder deflection
 X_u : Rate of change of surge force with surge velocity
 X, Y : Surge and sway forces
 U : Ship advance speed
 Y_r : Rate of change of sway force with yaw rate
 Y_u : Rate of change of sway force with surge velocity
 Y_{vu} : Rate of change of Y_u with sway velocity (coupled derivative)